Journal of the European Ceramic Society 40 (2020) 3600–3607

Contents lists available at ScienceDirect

Journal of the European Ceramic Society

journal homepage: www.elsevier.com/locate/jeurceramsoc

Original Article

Performance of borosilicate glass/$Ba_3(VO_4)_2$ ceramic composites and chemical stability with Ag electrodes

Haikui Zhu[a,b,*], Huidong Gu[a,b], Ye Dong[a,b], Wenjie Bian[a,b], Qitu Zhang[a,b]

[a] College of Materials Science and Engineering, Nanjing Tech University, Nanjing 211816, China
[b] Jiangsu Collaborative Innovation Center for Advanced Inorganic Function Composites, Nanjing 211816, China

ARTICLE INFO

Keywords:
Ceramic composites
Borosilicate glass/$Ba_3(VO_4)_2$
Dielectric properties
Cofiring
Chemical stability

ABSTRACT

In the present work, a systematic study on performance of borosilicate glass/$Ba_3(VO_4)_2$ ceramic composites synthesized by the traditional solid-state reaction method was conducted. Borosilicate glass is beneficial for reducing the sintering temperature of glass/$Ba_3(VO_4)_2$ ceramic composites below 900 °C due to the formation of a liquid phase. The ceramic composites with 35 %~40 % $Ba_3(VO_4)_2$ can effectively adjust the temperature coefficient of resonant frequency (τ_f) to approximately 0. The diffusion activation energy (Q_{Ag}) increases from 113.92 kJ/mol to 185 kJ/mol, as $Ba_3(VO_4)_2$ content increases from 0 to 40 % in the ceramic composites. A 0.65 borosilicate glass-0.35$Ba_3(VO_4)_2$ ceramic composite possesses excellent properties including an ε_r of 8.66, $Q \times f$ value of 20,338 GHz, the largest volume resistivity of 5.1 × 10^{13} Ω·cm and a flexural strength of 259 MPa. Ag exists only in the zero-valence state in the ceramic composite, and $Ba_3(VO_4)_2$ ceramic can block the diffusion channels and increase the barrier to the movement of Ag ions.

1. Introduction

Currently, with the development of science and technology, the excellent comprehensive performance of information communication systems is strongly required, and their functions are becoming more and more complex [1–3]. Among the incorporated components, passive components play key roles and determine the volume, weight, reliability and multifunction of wireless communication systems for modern higher-frequency fields [4–7]. To meet the needs of electronic information industry development, many integration technologies for passive electronic components [8,9] have emerged in recent decades, such as low-temperature cofired ceramic technology (LTCC), multi-chip module technology (MCM), chip packaging technology (CPS), etc. LTCC technologies, with a low-cost, high integration, excellent electrical characteristics and convenient process operations, have become the mainstream manufacturing method for the large-scale integration of electronic components [10–12].

As the basis of LTCC technology, LTCC materials are required to have a low sintering temperature (below 900 °C) for cofiring with Ag electrodes, a low dielectric constant and low dielectric loss for fast signal transmission, and they especially need to have a near-zero temperature coefficient of the resonator frequency (τ_f) for a stable working performance under different environmental conditions [13–15]. At present, the most popular and dominant LTCC products on the market are still focused on glass-based systems, i.e., glass ceramic or glass-filled ceramic [16,17], such as the $CaO-B_2O_3-SiO_2$ glass ceramic system of Ferro A6 and the lead borosilicate glass-filled Al_2O_3 system of DuPont 951. In addition to these, many glass-based LTCC materials have been widely explored due to their low sintering temperature and excellent performance. These glass systems include $K_2O-CaO-SrO-BaO-B_2O_3-SiO_2$ [18], $SnO-SnF_2-P_2O_5$ glass [19], $CaO-ZnO-B_2O_3-P_2O_5-TiO_2$ glass-ceramics [20], $BaO-Al_2O_3-SiO_2$ glass/Al_2O_3 [21], $CuO-ZnO-B_2O_3-Li_2O$ glass/Al_2O_3 [22], and $La_2O_3-B_2O_3-CaO-P_2O_5$ glass/cordierite composites [23]. However, there are still many problems [24,25] associated with these glass-based LTCC materials, which are becoming a huge barrier for further practical applications in the LTCC field, especially concerning the diffusion and chemical coexistence stability with Ag electrodes and the temperature coefficients that are too large.

To solve these specific problems, some methods have been developed. A straightforward method of suppression of the Ag diffusion is the formation of a composite or replacement for some constituents via different additions to enhance the crystallization or modify the structure. To address large temperature coefficients, the most effective method is composite sintering with an opposite τ_f value phase. Glass-based LTCC materials generally have negative τ_f values, which can tune τ_f to near zero by compensating with a positive τ_f material such as TiO_2, $CaTiO_3$ or $Ba_3(VO_4)_2$ [26–28]. It's well known that although TiO_2 and $CaTiO_3$ have high enough τ_f values, at approximately +450 ppm/°C

* Corresponding author at: College of Materials Science and Engineering, Nanjing Tech University, Nanjing 211816, China.
E-mail address: zhk@njtech.edu.cn (H. Zhu).

https://doi.org/10.1016/j.jeurceramsoc.2020.04.007
Received 7 February 2020; Received in revised form 30 March 2020; Accepted 3 April 2020
Available online 12 April 2020

and +800 ppm/°C, respectively, they still possess large dielectric constant values (> 100) [29,30]. By using TiO_2 and $CaTiO_3$ to improve τ_f, it is certain that the dielectric constant will be greatly increased. Among these positive τ_f materials, $Ba_3(VO_4)_2$ has a much lower dielectric constant of 14 and a positive τ_f of approximately 60 ppm/°C [31]. $Ba_3(VO_4)_2$ is particularly suitable as a near-zero τ_f-adjusting material, and examples include $BaMoO_4$-$Ba_3(VO_4)_2$ [32], (1-x)$Ca_5Mg_4(VO_4)_6$-x$Ba_3(VO_4)_2$ [33], (1-x)$Ba_3(VO_4)_2$- x$LiMg_{0.9}Zn_{0.1}PO_4$ [34], etc. However, $Ba_3(VO_4)_2$ can be completely densified at much higher temperatures (> 1100 °C), which are much higher than the melting point of Ag and limit the application of the material in the LTCC field. Many works have been performed to reduce the sintering temperature by adding low-melting additives or forming solid solutions [31,35]. However, these methods often bring about the deterioration of the τ_f value to a certain extent.

Borosilicate glass has been developed as one of the most promising materials for LTCC composite applications due to its low sintering temperature, excellent microwave dielectric properties, chemical reliability and low cost. The Borosilicate glass in ceramic composite may avoid several undesirable effects, such as the degradation of dielectric properties and chemical reaction with ceramics. However, there are few studies on the effects of $Ba_3(VO_4)_2$ in glass-based material systems on the phase composition, microstructure, temperature coefficient of the resonant frequency, diffusion inhibition and chemical compatibility with Ag electrodes. In this work, a borosilicate glass/$Ba_3(VO_4)_2$ ceramic composite was selected as the research system. $Ba_3(VO_4)_2$ ceramic is supposed to modify the temperature coefficient and inhibit Ag diffusion in the borosilicate glass, while borosilicate glass acts as the main liquid phase flux to reduce the sintering temperature of $Ba_3(VO_4)_2$ below 900 °C. Furthermore, the Ag diffusion, activation energy and chemical stability of borosilicate glass/$Ba_3(VO_4)_2$ ceramic composites were systematically investigated and discussed in detail. To the best of our knowledge, this relationship within the borosilicate glass/$Ba_3(VO_4)_2$ ceramic composite has not been reported in the literature thus far and provides a reliable basis for the popularization and application of this ceramic composite.

2. Experimental procedures

Borosilicate glass and $Ba_3(VO_4)_2$ ceramic were chosen as the raw materials in this work. The composition of the borosilicate glass powder was $8Al_2O_3$-22CaO-45SiO_2-22B_2O_3-3alkaline oxide (wt%). $Ba_3(VO_4)_2$ ceramic was prepared in a stoichiometric ratio using $BaCO_3$ (A.R., Sinoreagent Group Co. Ltd. Shanghai, China) and V_2O_5 (≥99 %, Funing Prost Non Ferrous Metals Co., Ltd, Jiangsu, China) and then calcined at 1100 °C for 4 h. (1-x)Borosilicate glass-x$Ba_3(VO_4)_2$ (x = 0, 0.20, 0.25, 0.30, 0.35 and 0.4, vol.%) glass ceramic samples were produced by the standard solid-state reaction process. First, the borosilicate glass and $Ba_3(VO_4)_2$ powders were mixed with ethanol and ball-milled for 12 h. After pan-drying, an 8 wt% polyvinyl alcohol solution was selected as the molding binder and added into the powder mixture. Then, granulation was carried out by grinding in a mortar to form small particles with a uniform size, which were pressed into disks with a size of approximately 13 mm in diameter and 5 mm in thickness under 100 MPa using a steel mold. Finally, these green bodies were heated from 850 °C to 925 °C for 1 h with a ZrO_2 load-bearing plate. Al_2O_3 powders of 1 μm in size were placed between the green compacts and bearing plate to prevent local bonding. The Ag metal electrode diffusion and chemical compatibility of the borosilicate glass/$Ba_3(VO_4)_2$ ceramic composite were investigated using specimens that were cofired with 5 wt% Ag nanoparticles or printed electrodes in the ambient atmosphere.

The density values of other specimens were determined by the Archimedes method. The crystalline-phase constituents and microstructures were characterized by X-ray diffraction (XRD, RigakuD/Max 2500 type, Japan) with Cu Kα radiation (k =0.15406 nm with a step size of 0.02 nm) and scanning electron microscopy (SEM, Hitachi SU8010, Japan), respectively. For SEM measurement, approximately 0.1 mm of the surface of each sintered specimen was ground off, polished and then thermally etched at 790 °C for 20 min. Chemical components were identified by energy-dispersive spectroscopy (EDS Vantage DS). The microwave dielectric properties of the samples were obtained by a network analyzer (Agilent E5071C, Malaysia) using the TE011 mode. The valence states of the elements in the borosilicate glass/$Ba_3(VO_4)_2$ ceramic composite were determined by X-ray photoelectron spectroscopy (XPS, Escalab 250 Xi, Thermo Fisher Scientific, US) with a monochromatic Al Kα radiation source. The thermal behavior was measured by a differential scanning calorimeter (DSC, Netzsch STA 449F3, Selb, Germany) using alumina as the standard object at a heating rate of 10 °C/min in air. The volume resistivity of the ceramic composite was tested by a high-resistance meter (HIOKI, SM7110, Nagano, Japan) at 100 V/DC. The coefficient of thermal expansion (CTE) of the sintered body was acquired using a high-performance thermal analyzer (RPZ-01) at a heating rate of 5 °C min^{-1} in the temperature range between 25 and 500 °C. The flexural strength of the sintered strip sample was obtained under a support distance of 30.0 mm using an electronic universal testing machine (CSS-2205) with a sample size of 40 mm × 4 mm × 3 mm and a support distance of 30.0 mm. The temperature coefficients of the resonant frequency (τ_f) values were measured from 20 °C to 80 °C and calculated according to Eq. 1 as follows:

$$\tau_f = \frac{f_1 - f_0}{f_0 \times (T_1 - T_0)} \quad (1)$$

where f_1 and f_0 are the resonant frequencies at the testing temperature T_1 of 80 °C and T_0 of 20 °C, respectively.

3. Results and discussion

Fig. 1 displays the XRD patterns of borosilicate glass and glass sintered at 875 °C for 1 h. The XRD patterns are mainly composed of the diffusion peak of an amorphous glassy phase, and there are no obvious crystals in the two glass specimens. Therefore, the heating process adopted in the experiment does not lead to a large amount of glass devitrification. The insert in Fig. 1 shows the DSC curve of borosilicate glass, which is measured in air from room temperature to 1000 °C. An endothermic peak is identified at 762 °C, which can be determined as the softening point of borosilicate glass. Therefore, borosilicate glass can be transformed into the liquid phase at 762 °C. Two exothermic peaks at 814 °C and 865 °C are also shown in the insert, which are attributed to glass crystallization. However, the borosilicate glass treated at 875 °C does not contain sharp crystalline peaks but shows only one low broad amorphous-phase peak. The results indicate that a

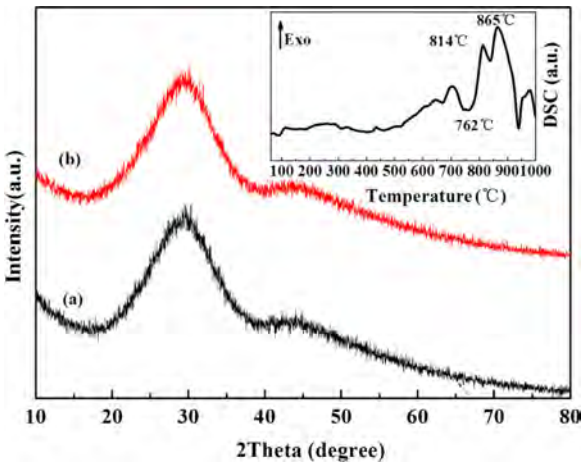

Fig. 1. XRD patterns of borosilicate glass samples: (a) glass and (b) sintered at 875 °C for 1 h. The insert is the DSC curve of borosilicate glass.

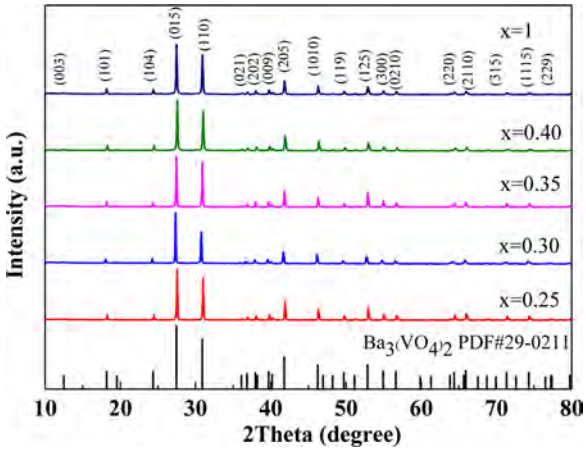

Fig. 2. XRD patterns of borosilicate glass/$Ba_3(VO_4)_2$ ceramic composites sintered at 875 °C for 1 h.

large number of microcrystals appear during the heat treatment. The microcrystals have an ordered structure in the short range and a disordered structure in the long range.

Fig. 2 shows the XRD patterns of borosilicate glass/$Ba_3(VO_4)_2$ ceramic samples sintered at 875 °C for 1 h. The sharp peaks appearing in the samples with x = 0.25–1 are identified as only a single phase of $Ba_3(VO_4)_2$ crystals with a rhombohedral structure that belongs to the space group R-3 m (no. 166). Meanwhile, it also displays that the $Ba_3(VO_4)_2$ phase in the ceramic composite has relatively good crystallinity and a well-ordered structure. Upon combining these results with those in Fig. 1, it is obvious that borosilicate glass does not react with $Ba_3(VO_4)_2$ ceramic to generate other new substance phases during the sintering process. This also illustrates that borosilicate glass has better chemical compatibility with $Ba_3(VO_4)_2$ ceramic in synthetic procedures.

Fig. 3 shows the SEM micrographs of the polished surfaces of borosilicate glass/$Ba_3(VO_4)_2$ ceramic composites sintered at 875 °C for 1 h. The microstructure of pure borosilicate glass without $Ba_3(VO_4)_2$ ceramic in Fig. 3 (a) shows a large amount of liquid phase morphology. Borosilicate glass is also beneficial for reducing the sintering temperature of $Ba_3(VO_4)_2$ to below 900 °C due to the formation of a liquid phase. As shown in Fig. 3(b)~(d), the viscous flow of flux makes the $Ba_3(VO_4)_2$ ceramic grains tightly agglomerate, and the glass liquid phase gradually decreases as the addition of $Ba_3(VO_4)_2$ ceramic increases. The borosilicate glass/$Ba_3(VO_4)_2$ ceramic samples with $0.3 \leq x \leq 35$ exhibit a recognizable morphology and discernible grain boundaries. The average $Ba_3(VO_4)_2$ grain size is approximately 2 μm. However, for composites with ceramics contents of up to 40 % (Fig. 3(d)), some abnormal-growth grains of the $Ba_3(VO_4)_2$ phase also appear, and the grains tend to be approximately 5 μm. Under this condition, it is quite difficult for the borosilicate glass phase to completely wrap the $Ba_3(VO_4)_2$ ceramic grains.

Fig. 4 shows the relationship between the bulk densities, dielectric properties, resistivities of the borosilicate glass/$Ba_3(VO_4)_2$ ceramic composites and the x values. The bulk density, resistivity and ε_r values slightly increase with the increase of the $Ba_3(VO_4)_2$ ceramic content from 20 % to 40 % at the same sintering temperature. The bulk density and ε_r of pure $Ba_3(VO_4)_2$ ceramic are approximately 5 g·cm^{-3} and 14 in this study, which are much higher than those of borosilicate glass, which are approximately 2.5 g·cm^{-3} and 5. Thus, the density and ε_r value of borosilicate glass/$Ba_3(VO_4)_2$ ceramic composites vary from 3 g·cm^{-3} to 3.28 g·cm^{-3} and from 7.92 to 9.07, respectively. The dielectric constant (ε_{com}) of borosilicate glass/$Ba_3(VO_4)_2$ ceramic composites can be predicted by the following the mixture rule:

$$\varepsilon_{com} = V_1 \times lg\varepsilon_1 + V_2 \times lg\varepsilon_2 \quad (2)$$

where ε_1 and ε_2 are the dielectric constant of borosilicate glass and $Ba_3(VO_4)_2$, V_1 and V_2 represent the volume fractions of borosilicate glass and $Ba_3(VO_4)_2$, respectively. Just as the Fig. 4 shown, the calculated relative dielectric constant is in good agreement with the experimental value. It indirectly indicates that borosilicate glass and $Ba_3(VO_4)_2$ ceramic are randomly distributed and chemical compatibility between the two phases. The amount of $Ba_3(VO_4)_2$ phase plays a key role in improving the volume resistivity of the borosilicate glass/$Ba_3(VO_4)_2$ ceramic. The volume resistivity values improve from 1.2 × 10^{13} Ω·cm to 5.1 × 10^{13} Ω·cm upon increasing x from 0.2 to 0.35. Meanwhile, the Q × f values of the ceramic composites are kept between 18,320 GHz and 20,354 GHz, which are independent of the $Ba_3(VO_4)_2$ content. However, as shown in Fig. 3(d), for the samples containing as high as 40 % $Ba_3(VO_4)_2$ ceramic, the liquid phase has difficulty completely covering the $Ba_3(VO_4)_2$ grains, and some abnormal growth of $Ba_3(VO_4)_2$ grains also appears. In this case, the coordination and structural consistency between the borosilicate glass phase and $Ba_3(VO_4)_2$ ceramic phase are destroyed, which eventually gives rise to a deteriorated performance of the ceramic composite. In general, the 0.65borosilicate glass-0.35$Ba_3(VO_4)_2$ ceramic composite exhibits a better dielectric performance, with an ε_r of 8.66, a Q × f value of 20,338 GHz and the largest volume resistivity of 5.1 × 10^{13} Ω·cm.

Fig. 5 presents the τ_f variation trend of borosilicate glass/$Ba_3(VO_4)_2$ ceramic composites. The theoretical τ_f values of borosilicate glass/$Ba_3(VO_4)_2$ ceramic composites can be obtained by the following the mixture rule:

$$\tau_f = V_1 \times \tau_{f1} + V_2 \times \tau_{f2} \quad (3)$$

where τ_{f1} and τ_{f2} are the τ_f of borosilicate glass and $Ba_3(VO_4)_2$, V_1 and V_2 represent the volume fractions of borosilicate glass and $Ba_3(VO_4)_2$, respectively. The variation trend and values of theoretical τ_f are also in good agreement with the measured values. It can be obviously seen that $Ba_3(VO_4)_2$ ceramic can effectively adjust the τ_f values of borosilicate glass to approximately 0. The τ_f values monotonously increase from -18 ppm/°C (x = 0.2) to -1.7 ppm/°C (x = 0.35), after which the increasing range decreases (x > 0.35) and the τ_f value reaches 0.4.

The coefficients of thermal expansion (CTE) and flexural strengths of borosilicate glass/$Ba_3(VO_4)_2$ ceramic composites sintered at 875 °C for 1 h are shown in Fig. 6. The changing trend between the CTE, flexural strength value and $Ba_3(VO_4)_2$ content in the composites is a basically linear relationship. As the $Ba_3(VO_4)_2$ ceramic increases from 20 % to 40 %, the CTE values slightly vary from 6.8 × 10^{-6}/°C to 7.2 × 10^{-6}/°C and are somewhat independent of the $Ba_3(VO_4)_2$ content. However, it is obvious that composites with high $Ba_3(VO_4)_2$ contents show much larger flexural strengths. Compared to the sample containing 20 % $Ba_3(VO_4)_2$, the amplitude of the flexural strength increases by approximately 30 % from 202 MPa to 259 MPa upon the addition of 35 % $Ba_3(VO_4)_2$. $Ba_3(VO_4)_2$ ceramic grains can be considered to be particle toughening materials in the composites. For borosilicate glass, as a typical brittle material, it is easy for forces to travel in one direction through cracks. Just as the insert in Fig. 6 shows, the borosilicate glass/$Ba_3(VO_4)_2$ composite displays a dense sintering characteristic. When force is applied to the ceramic composite, the stress is quickly transferred to the ceramic particle surfaces and deflected toward all directions. It also causes microcrack deflection, dispersion, passivation, pinning, etc., which change the microcracks from unidirectional propagation into an overall stress state. When the $Ba_3(VO_4)_2$ content is 40 % (Fig. 3(d)), the glass phase is not enough to completely cover the $Ba_3(VO_4)_2$ ceramic grains, and some abnormally grown grains also emerge. This leads to a slight reduction in the flexural strength of the borosilicate glass/$Ba_3(VO_4)_2$ ceramic composite.

At present, Ag is the most promising and widely used metal electrode material for the LTCC process. It has been reported in some open literature [36–38] that if Ag diffusion occurs during the cofiring process, the performance and reliability of the materials will be greatly

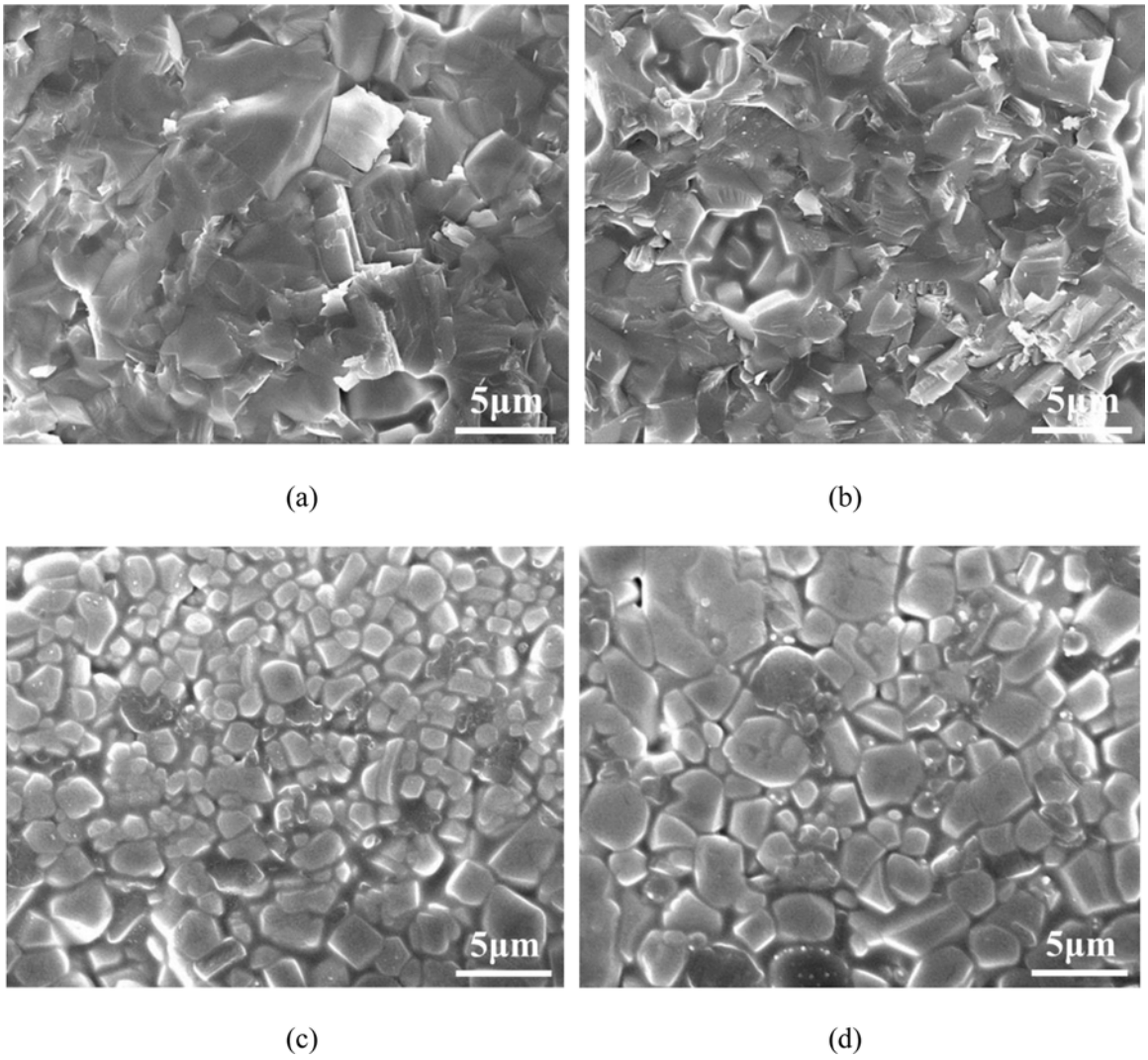

Fig. 3. SEM images of borosilicate glass/$Ba_3(VO_4)_2$ ceramic composites sintered at 875 °C for 1 h: (a) x = 0, (b) x = 0.30, (c) x = 0.35 and (d) x = 0.40.

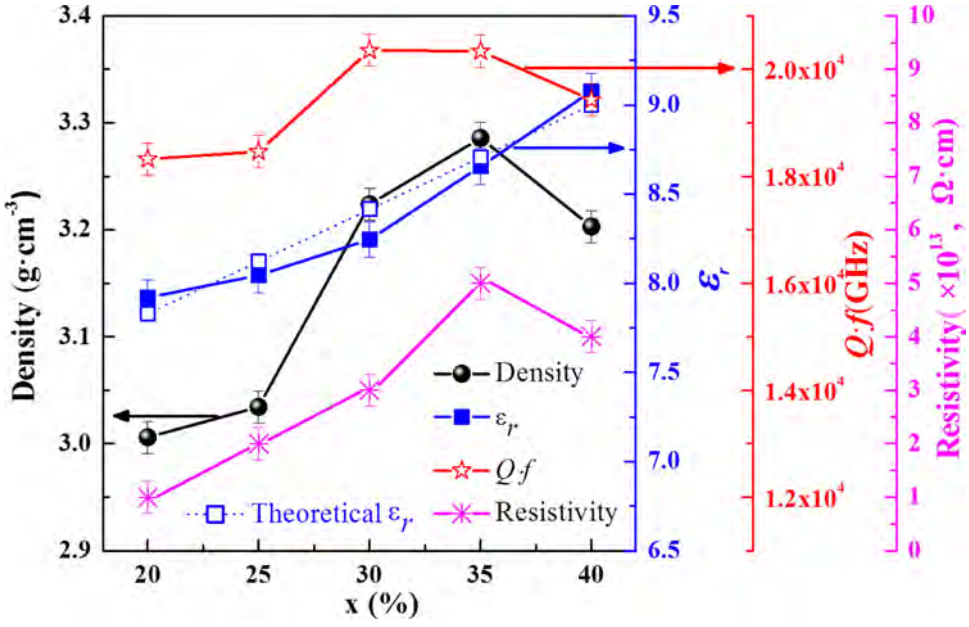

Fig. 4. The relationship between the bulk densities, dielectric properties, resistivity of the borosilicate glass/$Ba_3(VO_4)_2$ ceramic composites and the x values.

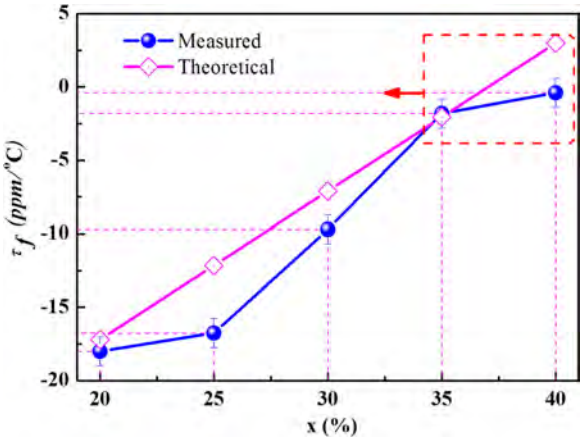

Fig. 5. τ_f values of borosilicate glass/$Ba_3(VO_4)_2$ ceramic composites.

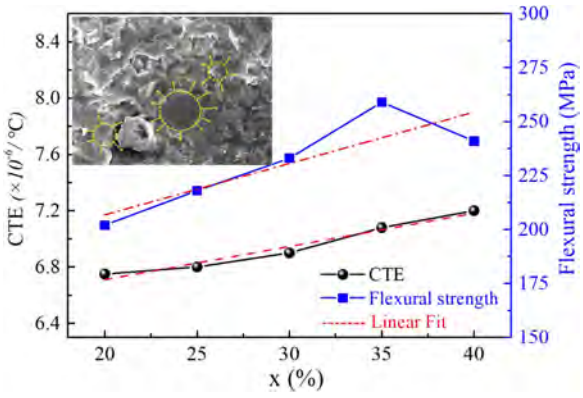

Fig. 6. CTE and flexural strength of the borosilicate glass/$Ba_3(VO_4)_2$ ceramic composite. The insert shows an SEM image and stress diagram of the borosilicate glass/$Ba_3(VO_4)_2$ composite.

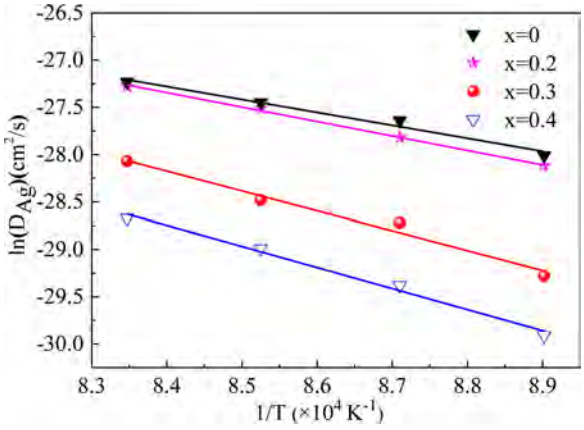

Fig. 7. The linear relationship between ln(D_{Ag}) values and 1/T.

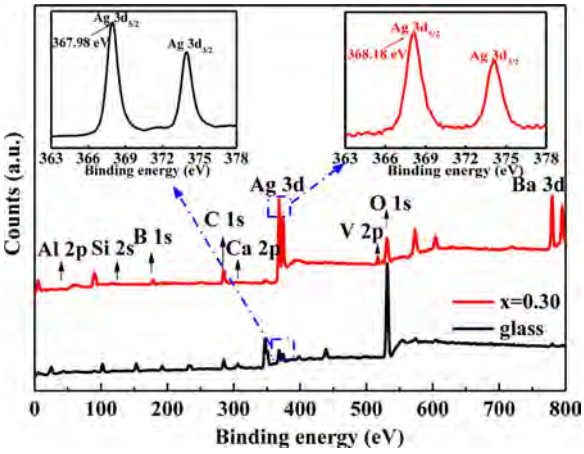

Fig. 8. XPS spectra of borosilicate glass and borosilicate glass/$Ba_3(VO_4)_2$ ceramic composite cofired with 5 wt% Ag powder.

reduced by effects such as reducing the insulation resistance and increasing the leakage current. Thus, it is urgent to explore the diffusion process and chemical reaction mechanism between the borosilicate glass/$Ba_3(VO_4)_2$ ceramic composite and Ag electrodes for practical applications. The degree of difficulty of Ag diffusion in borosilicate glass/$Ba_3(VO_4)_2$ ceramic composites can be characterized by the diffusion activation energy (Q_{Ag}). The average diffusion coefficient of Ag (D_{Ag}) in the borosilicate glass/$Ba_3(VO_4)_2$ ceramic composite can be obtained by the following equation [39,40]:

$$\frac{C_{Ag}(x, t)}{C_{Ag}} = 1 - erf\left[\frac{x}{2\sqrt{D_{Ag}t}}\right] \quad (4)$$

where *erf* refers to the error function, C_{Ag} is the initial silver content with a value of 100 %, C_{Ag} *(x,t)* is the Ag content at different positions in the vertical direction from the initial Ag electrode, and *t* in this study is 1 h. Then, the Q_{Ag} value can be calculated according to the following Arrhenius equation [41]:

$$D_{Ag} = D_0 \exp\left(-\frac{Q_{Ag}}{RT}\right) \quad (5)$$

where D_0 and R are described as a pre-exponential factor and a gas constant of 8.31 J/(mol K, respectively. It can be obviously seen from formula (5) that the logarithm of the diffusion coefficient is linear with the reciprocal of the temperature. As shown in Fig. 7, the slope of the linear fitting line is the diffusion activation energy. The Q_{Ag} values of ceramic composites containing 0, 20 %, 30 % and 40 % $Ba_3(VO_4)_2$ are 113.92 kJ/mol, 127.26 kJ/mol, 174.12 kJ/mol and 185 kJ/mol, respectively. $Ba_3(VO_4)_2$ ceramics play an obvious barrier role in borosilicate glass/$Ba_3(VO_4)_2$ ceramic composites and improve the diffusion activation energy of Ag.

Fig. 8 shows the XPS spectra of borosilicate glass and 0.7borosilicate glass-0.3$Ba_3(VO_4)_2$ ceramic composite cofired with 5 wt% Ag powders sintered at 875°C for 1 h. The peaks of all elements in the XPS spectra are verified by the standard C 1s peak value at 284.8 eV. The valence states of Ba, V, Al, Si, B, O and Ag are given in the measurement spectrum of Fig. 8, and the two inserts are enlarged portions of the XPS results of the Ag 3d peaks. The peak values of $Ag3d_{5/2}$ in borosilicate glass and 0.7borosilicate glass-0.3$Ba_3(VO_4)_2$ ceramic composite are 367.98 eV and 368.18 eV, respectively. The binding energies of the $Ag3d_{5/2}$ peaks for elemental silver, monovalent silver oxide and divalent silver oxide can be determined to be 368.20 eV, 367.70 eV and 367.40 eV, respectively [42,43]. The $Ag3d_{5/2}$ value of 367.98 eV in borosilicate glass is much closer to that of monovalent silver oxide. This implies that the Ag electrode can diffuse and react with some ingredients in the borosilicate glass, which causes monovalent and zero-valent silver to coexist. It can be seen from Fig. 7 that the diffusion activation energy of the ceramic composite significantly increases from 113.92 kJ/mol to 174.12 kJ/mol when the $Ba_3(VO_4)_2$ content is increased to 30 % $Ba_3(VO_4)_2$. This can increase the difficulty of silver diffusion and then sharply reduce the probability of chemical reaction. Therefore, Ag exists only in the zero-valence state in the borosilicate glass/$Ba_3(VO_4)_2$ ceramic composite sample, which means that the ceramic composite is stable with Ag powder during the cofiring process.

For a deeper understanding of the Ag diffusion and reaction behaviors, a schematic illustration of different sintering stages of the borosilicate glass and glass/$Ba_3(VO_4)_2$ ceramic composite is displayed in Fig. 9. Borosilicate glass and Ag are uniformly mixed and pressed into

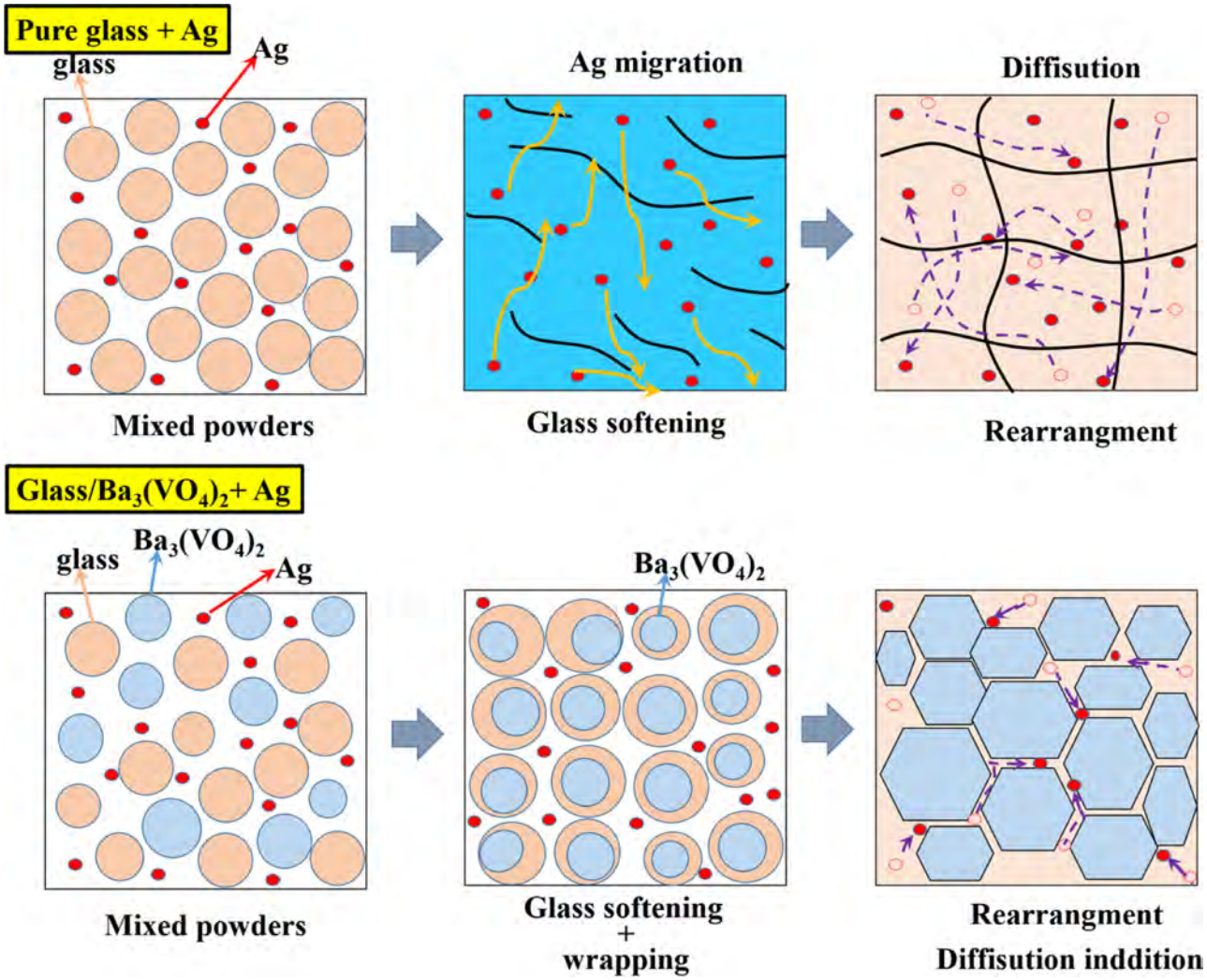

Fig. 9. Schematic diagram of the Ag diffusion and reaction behaviors at different sintering stages in borosilicate glass and glass/$Ba_3(VO_4)_2$ ceramic composite, respectively.

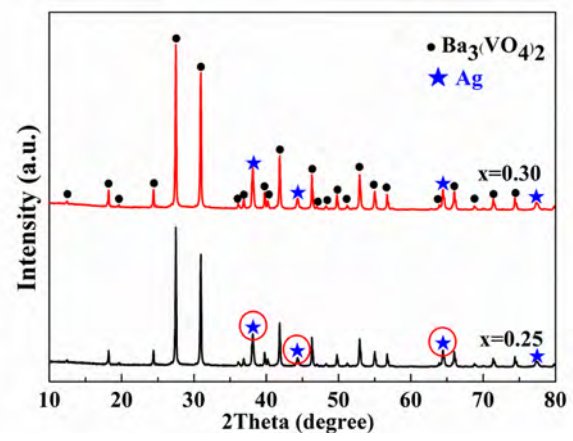

Fig. 10. X-ray diffraction patterns of Borosilicate glass/$Ba_3(VO_4)_2$ ceramic composite cofired with 5 wt% Ag powders.

shape, followed by heating to approximately 760 °C. Borosilicate glass gradually softens and begins to change into a liquid phase at this temperature, which gives rise to a viscous flow in the glassy phase. It was obvious that the dramatic reduction of the viscosity in the glass phase will be the driving force behind Ag diffusion [44]. Under this condition, Ag migration is much easier than that in glass solids, and the diffusion intensifies with the increase of the liquid phase [45]. Afterwards, the temperature gradually rises much higher, and the liquid glass phase promotes particles to become a sintered compact, while part of the Ag particles can move and melt into the glass matrix to form some univalent Ag compounds. This is the reason why the binding energy of the $Ag3d_{5/2}$ peak in borosilicate glass in Fig. 8 is only 367.98 eV. However, for the glass/$Ba_3(VO_4)_2$ ceramic composite, the liquid glass phase gradually fills the gaps between $Ba_3(VO_4)_2$ ceramic and wraps particles when the sintering temperature is higher than 760 °C. As the sintering temperature continuously rises, the solid surface of the $Ba_3(VO_4)_2$ powder partially decomposes and rearranges with the assistance of the liquid glass phase. With growth of the $Ba_3(VO_4)_2$ crystals, the grain boundary is slowly formed, and the glass phase exists only in the grain boundaries between grains. These phenomena can be clearly seen in Fig. 3(c) and (d). The network in the glass phase is destroyed, and the channels of Ag diffusion are naturally blocked. Based on the results in Fig. 7, 30 % $Ba_3(VO_4)_2$ ceramic in borosilicate glass can dramatically increase the diffusion activation energy from 113.92 kJ/mol to 174.12 kJ/mol. It can increase the barrier to the movement of Ag ions, and then, the diffusion quantity of Ag ions will sharply decrease.

The chemical stability of borosilicate glass/$Ba_3(VO_4)_2$ ceramic composite and Ag can also be seen from the XRD results, which are presented in Fig. 10. The XRD patterns in Fig. 10 are mainly composed of $Ba_3(VO_4)_2$ and Ag phase, which indicates that there is no change of

the main crystalline phase in the ceramic composite during the sintering process with Ag. Obviously, this result is consistent with the XPS spectral result shown in Fig. 8. It further illustrates that borosilicate glass and $Ba_3(VO_4)_2$ are able to exert their own advantages and complement each other's shortcomings in performance. It also enables the ceramic composite to be chemically stable with silver and coexist in the LTCC process.

4. Conclusions

The phase evolution, crystallization and sintering behaviors, and microwave dielectric properties of borosilicate glass/$Ba_3(VO_4)_2$ ceramic composites as well as their chemical stability on Ag electrodes were investigated. Borosilicate glass is beneficial for reducing the sintering temperature of glass/$Ba_3(VO_4)_2$ ceramic composites below 900 °C owing to the formation of a liquid phase. The ceramic composites with 35 %～40 % $Ba_3(VO_4)_2$ can effectively adjust the temperature coefficient of resonant frequency (τ_f) to approximately 0. The diffusion activation energy (Q_{Ag}) increases from 113.92 kJ/mol to 185 kJ/mol, as $Ba_3(VO_4)_2$ content increases from 0 to 40 % in the ceramic composites. An 0.65borosilicate glass-0.35$Ba_3(VO_4)_2$ ceramic possesses excellent properties—an ε_r of 8.66, Q × f value of 20,338 GHz, the largest volume resistivity of 5.1 × 10^{13} Ω·cm and a flexural strength of 259 MPa. Borosilicate glass/$Ba_3(VO_4)_2$ ceramic composites can obviously inhibit silver diffusion and limit its reaction during the cofiring process, which lays a solid foundation for the practical application of this ceramic composite in LTCC basic components.

Declaration of Competing Interest

The authors declare that they have no known competing financial interests or personal relationships that could have appeared to influence the work reported in this paper.

Acknowledgments

This work was supported by the Priority Academic Program Development of Jiangsu Higher Education Institutions (PAPD), the Jiangsu Collaborative Innovation Center for Advanced Inorganic Function Composites, and the Top-notch Academic Programs Project of Jiangsu Higher Education Institutions (TAPP, PPZY2015B128).

References

[1] H.F. Zhou, K.G. Wang, W.D. Sun, X.L. Chen, H. Ruan, Phase composition, singtering behavior and microwave dielectric properties of $M_2BiLi_2V_3O_{12}$ (M = Zn, Ca) low temperature co-fired ceramics, Mater. Lett. 217 (2018) 20–22.
[2] A.N. Unnimay, E.K. Suresh, R. Ratheesh, Crystal structure and microwave dielectric properties of new alkaline earth vanadate $A_4V_2O_9$ (A = Ba, Sr, Ca, Mg and Zn) ceramics for LTCC applications, Mater. Res. Bull. 88 (2017) 174–181.
[3] F. Xie, L.J. Jia, F. Xu, G.W. Gan, J. Li, Y.L. Li, Y.X. Li, H.W. Zhang, Low-temperature sintering LiZnTiMn ferrite ceramics: synthesis, microstructure, and enhanced ferromagnetic properties with CuO-V_2O_5 additive, J. Mater. Sci.-Mater. Electron. 29 (15) (2018) 13337–13344.
[4] G.X. Shen, W.Q. Che, Q. Xue, Compact microwave and millimeter-wave bandpass filters using ltcc-based hybrid lumped and distributed resonators, IEEE Access 7 (2019) 104797–104809.
[5] D.S. Wu, Y.C. Li, Q. Xue, Filtering power divider with harmonic suppression based on LTCC broadside coupling, Electron. Lett. 54 (11) (2019) 697–698.
[6] Y.C. Lee, C.S. Park, LTCC-based monolithic system-in-package (SiP) module for millimeter-wave applications, Int. J. Rf. Microw. C. E. 26 (9) (2016) 803–811.
[7] B. Synkiewicz-Musialska, D. Szwagierczak, J. Kulawik, N. Palka, P.R. Bajurko, Impact of additives and processing on microstructure and dielectric properties of willemite ceramics for LTCC terahertz applications, J. Eur. Ceram. Soc. 40 (2) (2020) 362–370.
[8] G. Dong, W. Xiong, Z.Y. Wu, Y.T. Yang, Antenna-in-package system integrated with meander line antenna based on LTCC technology, Front. Inf. Technol. Electron. Eng. 17 (1) (2016) 67–73.
[9] D. Wilcox, R.F. Huang, S.X. Dai, Enabling materials for wireless multilayer ceramic integrated circuit (MCIC) applications, Ceram. Trans. 97 (1999) 201–213.
[10] M.T. Sebastian, H. Jantunen, Low loss dielectric materials for LTCC applications: a review, Int. Mater. Rev. 53 (2008) 57–90.
[11] A. Surjith, R. Ratheesh, High Q ceramics in the $ACe_2(MoO_4)_4$ (A = Ba, Sr and Ca) system for LTCC applications, J. Alloys. Compd. 550 (2013) 169–172.
[12] T.K. Gupta, J.H. Jean, Principles of the development of a silica dielectric for microelectronics, J. Mater. Res. 11 (1996) 243–263.
[13] H.I. Hsiang, C.S. Hsi, C.C. Huang, S.L. Fu, Sintering behavior and dielectric properties of $BaTiO_3$ ceramics with glass addition for internal capacitor of LTCC, J. Alloys. Compd. 459 (1–2) (2008) 307–310.
[14] A. Bittner, H. Seidel, U. Schmid, Electromigration resistance and long term stability of textured silver thin films on LTCC, Microelectron. Eng. 88 (1) (2011) 127–130.
[15] H.S. Ren, L. Hao, H.Y. Peng, M.Z. Danga, T.Y. Xie, Y. Zhang, S.H. Jiang, X.G. Yao, H.X. Lin, L. Luo, Investigation on low-temperature sinterable behavior and tunable dielectric properties of BLMT glass-$Li_2ZnTi_3O_8$ composite ceramics, J. Eur. Ceram. Soc. 38 (2018) 3498–3504.
[16] Doruk M.üftüoglu Ali Hajian, Thomas Konegger, Michael Schneider Ulrich Schmid, On the porosification of LTCC substrates with sodium hydroxide, Compos. Part. B. Eng. 157 (2019) 14–23.
[17] L.P. Yu, S.S. Qi, Z.S. Ma, R.Z. Zuo, Experimental determination of the uniaxial viscosity of low-temperature co-fired ceramic tapes by vertical sintering, Ceram. Int. 40 (7) (2014) 9367–9375.
[18] J.H. Jean, Y.C. Fang, S.X. Dai, Devitrification kinetics and mechanism of K_2O-CaO-SrO-BaO-B_2O_3-SiO_2 glass-ceramic, J. Am. Ceram. Soc. 100 (2017) 2632–2640.
[19] Indira J. Induja, Mailadil T. Sebastian, Microwave dielectric properties of SnO-SnF_2-P_2O_5 glass and its composite with alumina for ULTCC applications, J. Am. Ceram. Soc. 84 (6) (2001) 1354–1360.
[20] D.H. Jiang, J.J. Chen, B.B. Lu, J. Xi, F. Shang, J.W. Xu, Preparation, crystallization kinetics and microwave dielectric properties of CaO-ZnO-B_2O_3-P_2O_5-TiO_2 glass-ceramics, Ceram. Int. 45 (2019) 8233–8237.
[21] H.J. Mao, X.Y. Chen, F.L. Wang, W.J. Zhang, Effects of alkaline earth oxides on the densification and microwave properties of low-temperature fired BaO-Al_2O_3-SiO_2 glass-ceramic/Al_2O_3 composites, J. Mater. Sci. 54 (19) (2019) 12371–12380.
[22] J. Xi, G.H. Chen, F. Liu, F. Shang, J.W. Xu, C.R. Zhou, C.L. Yuan, Synthesis, microstructure and characterization of ultra-low permittivity CuO-ZnO-B_2O_3-Li_2O glass/Al_2O_3 composites for ULTCC application, Ceram. Int. 45 (18) (2019) 24431–24436.
[23] F.L. Wang, W.J. Zhang, X.Y. Chen, H.J. Mao, Synthesis and characterization of low CTE value La_2O_3-B_2O_3-CaO-P_2O_5 glass/cordierite composites for LTCC application, Ceram. Int. 45 (2019) 7203–7209.
[24] M. Valant, D. Suvorov, Chemical compatibility between silver electrodes and Low-Firing Binary-Oxide compound, J. Am. Ceram. Soc. 83 (11) (2010) 2721–2729.
[25] A. Bittner, N. Pagel, H. Seidel, U. Schmid, Long-term stability of Ag and Cu thin films on glass, LTCC and alumina substrates, Microsyst. Technol. 18 (2012) 879–884.
[26] S.Y. Cho, H.J. Youn, H.J. Lee, K.S. Hong, Contribution of structure to temperature dependence of resonant frequency in the (1-x)$La(Zn_{1/2}Ti_{1/2})O_3$·x$ATiO_3$ (A = Ca, Sr) System, J. Am. Ceram. Soc. 84 (4) (2010) 753–758.
[27] C.Z. Yin, C.C. Li, G.J. Yang, L. Fang, Y.H. Yuan, L.L. Shu, J. Khaliq, $NaCa_4V_5O_{17}$: A low-firing microwave dielectric ceramic with low permittivity and chemical compatibility with silver for LTCC applications, J. Eur. Ceram. Soc. 40 (2020) 386–390.
[28] J. Zhang, R.Z. Zuo, J. Song, Y.D. Xu, M. Shi, Low-loss and low-temperature firable Li2Mg_3SnO_6-$Ba_3(VO_4)$2 microwave dielectric ceramics for LTCC applications, Ceram. Int. 44 (2) (2018) 2606–2610.
[29] D. Thomas, M.T. Sebastian, Temperature-compensated $LiMgPO_4$: A new glass-free low-temperature cofired ceramic, J. Am. Ceram. Soc. 93 (11) (2010) 3828–3831.
[30] C.L. Huang, M.H. Weng, Improved high q value of $MgTiO_3$-$CaTiO_3$ microwave dielectric ceramics at low sintering temperature, Mater. Res. Bull. 36 (15) (2001) 2741–2750.
[31] R. Umemura, H. Ogawa, A. Yokoi, H. Ohsato, A. Kan, Low temperature sintering-microwave dielectric property relations in $Ba_3(VO_4)_2$ ceramic, J. Alloys. Compd. 424 (2006) 388–393.
[32] C.F. Min, H.K. Zhu, Y. Wang, Q.T. Zhang, F.Q. Yan, X. Wang, Preparation and microwave dielectric properties of $BaMoO_4$-$Ba_3(VO_4)_2$ ceramic composites, J. Mater. Sci. Mater. Electron. 30 (2019) 9507–9512.
[33] G.G. Yao, C.J. Pei, H. Ma, J.G. Xu, P. Liu, H.W. Zhang, Low-temperature firing and microwave dielectric properties of (1-x)$Ca_5Mg_4(VO_4)_6$-x$Ba_3(VO_4)_2$ temperature stable ceramics, J. Alloys. Compd. 709 (2017) 234–239.
[34] Y. Lv, R.Z. Zuo, Y. Cheng, C. Zhang, Low-temperature sinterable (1-x)$Ba_3(VO_4)_2$-x$LiMg_{0.9}Zn_{0.1}PO_4$ microwave dielectric ceramics, J. Am. Ceram. Soc. 96 (2013) 3862–3867.
[35] Z.Y. Zhang, H.K. Zhu, Y.Y. Li, L. Li, Z.X. Fu, K. Huang, Q.T. Zhang, Low temperature sintering and dielectric properties of $Ba_3(VO_4)_2$ microwave ceramics using Co_2O_3 additives, J. Mater. Sci. Mater. Electron. 28 (2017) 18474–18479.
[36] K.B. Shim, N.T. Cho, S.W. Lee, Silver diffusion and microstructure in LTCC multilayer couplers for high frequency applications, J. Mater. Sci. 35 (2000) 813–820.
[37] J.H. Jean, C.R. Chang, C.D. Lei, Sintering of a crystallizable CaO-B_2O_3-SiO_2 glass with silver, J. Am. Ceram. Soc. 87 (2004) 1244–1249.
[38] C.S. Hsi, Y.R. Chen, H.I. Hsiang, Diffusivity of silver ions in the low temperature co-fired ceramic (LTCC) substrates, J. Mater. Sci. Mater. 46 (2011) 4695–4700.
[39] M. Ma, Z. Liu, F. Zhang, L. Feng, Y. Li, Suppression of silver diffusion in borosilicate glass-based low-temperature cofired ceramics by copper oxide addition, J. Am. Ceram. Soc. 99 (7) (2016) 2402–2407.
[40] J.H. Jean, C.R. Chang, Interfacial reaction kinetics between silver and ceramic-filled glass substrate, J. Am. Ceram. Soc. 87 (2004) 1287–1293.
[41] S. Kobayashi, T. Yakou, Control of intermetallic compound layers at interface between steel and aluminum by diffusion-treatment, Mater. Sci. Eng. A 338 (2002) 44–53.
[42] J.M. Hollander, W.L. Jolly, X-ray Photoelectron Spectroscopy, (1970).

[43] G.B. Hoflund, Z.F. Hazos, G.N. Salaita, Surface characterization study of Ag, AgO, and Ag_2O using x-ray photoelectron spectroscopy and electron energy-loss spectroscopy, Phys. Rev. B 62 (2000) 11126–11133.
[44] Y.T. Shih, J.H. Jean, S.C. Lin, Failure mechanism of a low-temperature-cofired ceramic capacitor with an inner ag electrode, J. Am. Ceram. Soc. 93 (2010) 3278–3283.
[45] M. Prudenziati, B. Morten, A.F. Gualtieri, M. Leoni, Dissolution kinetics and diffusivity of silver in glassy layers for hybrid microelectronics, J. Mater. Sci: Mater. Electron. 15 (2004) 447–453.